Supporting Information

Composition Control of Alloy Nanoparticles Consisting of Bulk-Immiscible Au and Rh Metals via an Ionic Liquid/Metal Sputtering Technique for Improving Their Electrocatalytic Activity

Kazutaka Akiyoshi,[a] Yumezo Watanabe,[a] Tatsuya Kameyama,[a] Tokuhisa Kawawaki,[b,c] Yuichi Negishi,[b,c], Susumu Kuwabata,[d] and Tsukasa Torimoto*[a]

[a] Graduate School of Engineering, Nagoya University, Furo-cho, Chikusa-ku, Nagoya 464-8603, Japan. E-mail: torimoto@apchem.nagoya-u.ac.jp

[b] Department of Applied Chemistry, Faculty of Science, Tokyo University of Science, Kagurazaka, Shinjuku-ku, Tokyo 162-8601, Japan.

[c] Research Institute for Science and Technology, Tokyo University of Science, Kagurazaka, Shinjuku-ku, Tokyo 162-8601, Japan.

[d] Graduate School of Engineering, Osaka University, 2-1 Yamada-oka, Suita, Osaka 565-0871, Japan.

E-mail: torimoto@chembio.nagoya-u.ac.jp

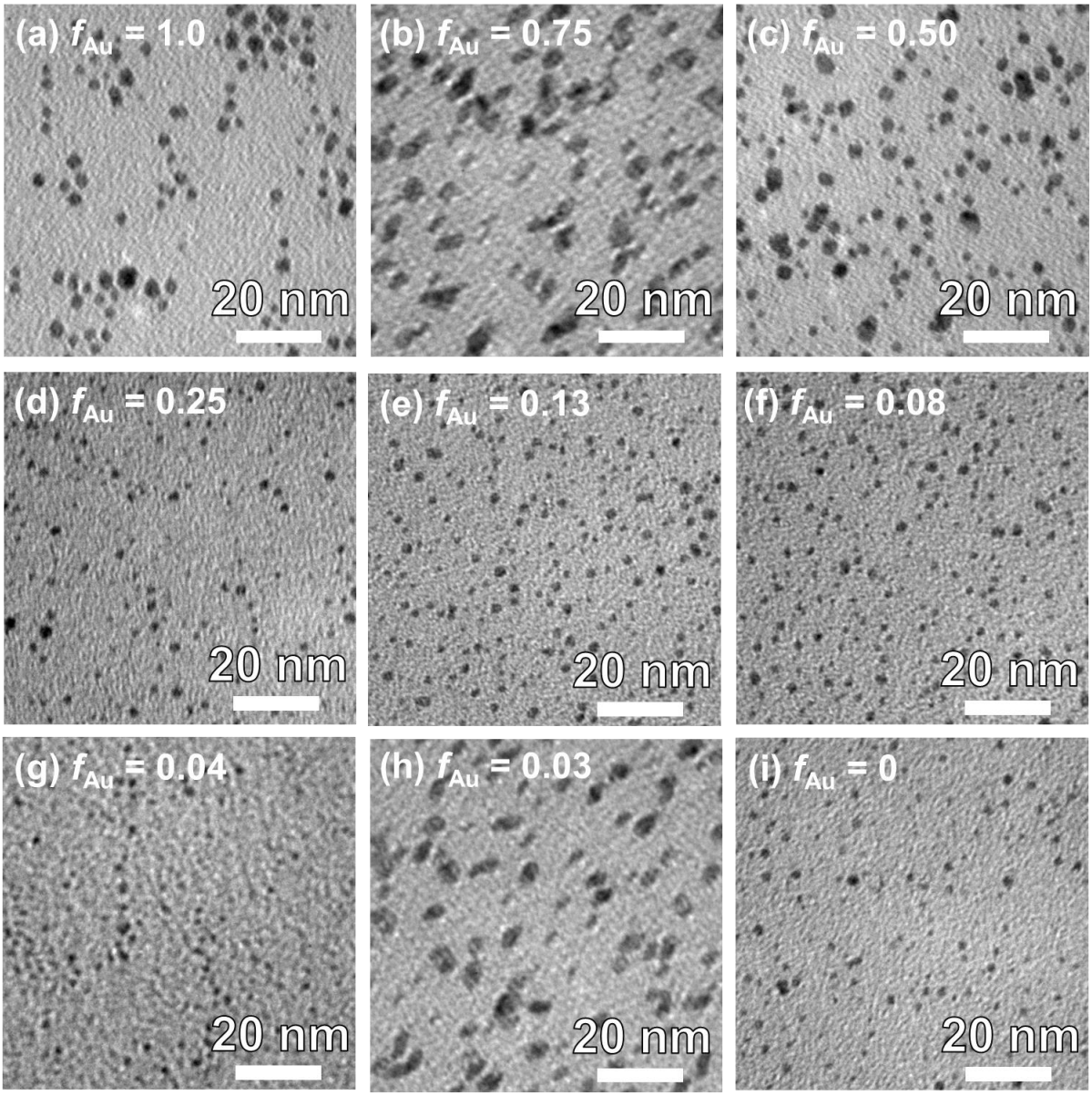

Figure S1. TEM images of sputter-deposited Au, AuRh, and Rh NPs. The samples were Au NPs (f_{Au} = 1.0) (a), AuRh NPs (f_{Au} = 0.75) (b), (f_{Au} = 0.50) (c), (f_{Au} = 0.25) (d), (f_{Au} = 0.13) (e), (f_{Au} = 0.08) (f), (f_{Au} = 0.04) (g), (f_{Au} = 0.03) (h), and Rh NPs (f_{Au} = 0) (i).

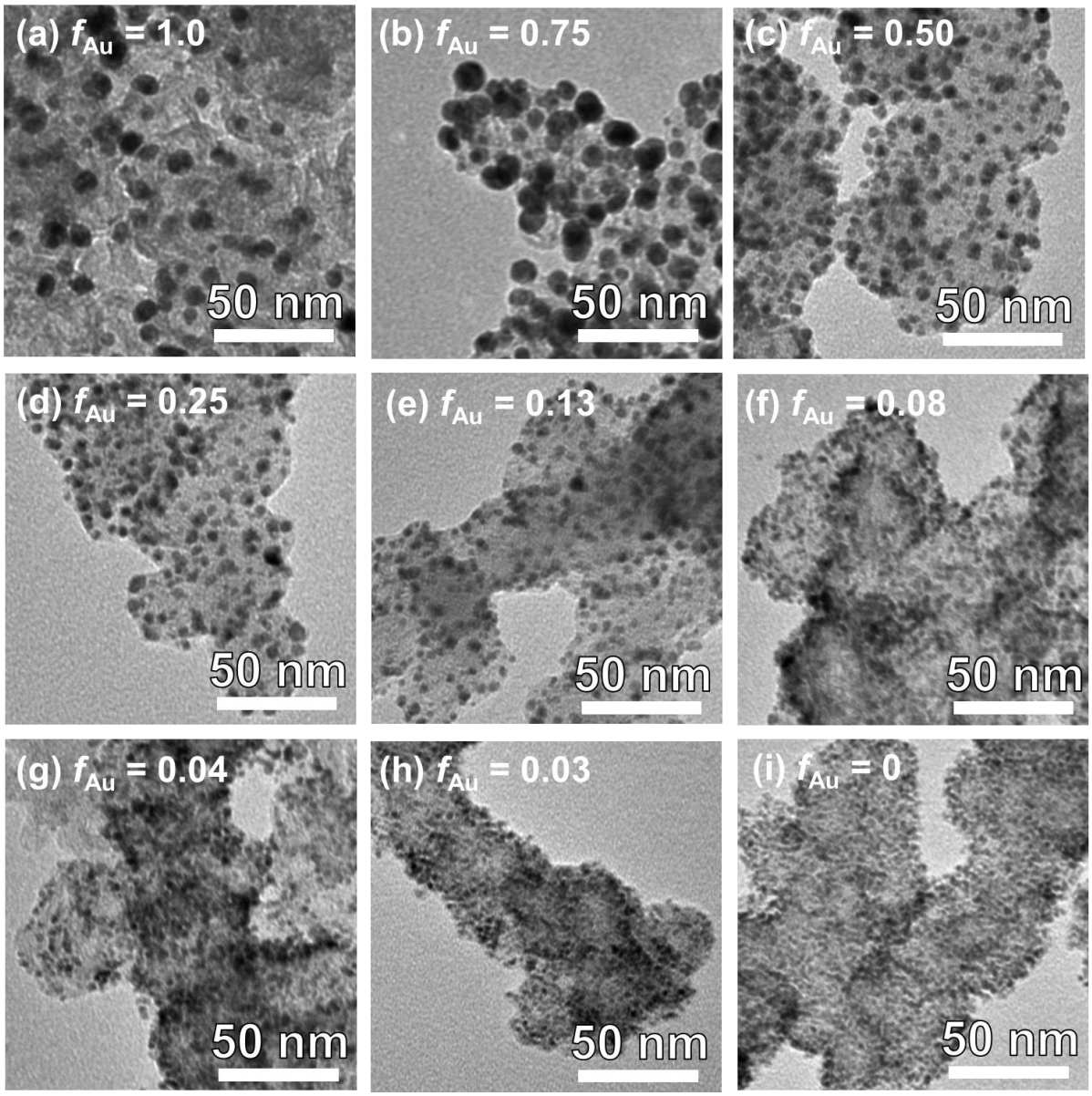

Figure S2. TEM images of Au/CB, AuRh/CB, and Rh/CB catalysts. The samples were Au/CB (f_{Au} = 1.0) (a), $Au_{99}Rh_1$/CB (f_{Au} = 0.75) (b), $Au_{91}Rh_9$/CB (f_{Au} = 0.50) (c), $Au_{73}Rh_{27}$/CB (f_{Au} = 0.25) (d), $Au_{59}Rh_{41}$/CB (f_{Au} = 0.13) (e), $Au_{44}Rh_{56}$/CB (f_{Au} = 0.08) (f), $Au_{27}Rh_{73}$/CB (f_{Au} = 0.04) (g), $Au_{23}Rh_{77}$/CB (f_{Au} = 0.03) (h), and Rh/CB (f_{Au} = 0) (i).

Table S1. Crystalline sizes of AuRh NPs loaded on CB particles, determined from the widths of 111 diffraction peaks in XRD patterns with use of Scherrer's equation.

Sample	Peak position of 111 diffraction [degree]	FWHM [degree]	Crystalline size [nm]	NP size from TEM [nm][a]
Au/CB	38.19	0.174	50.6	8.8
$Au_{99}Rh_1$/CB	38.20	0.302	29.1	6.3
$Au_{91}Rh_9$/CB	38.60	0.705	12.5	3.2
$Au_{73}Rh_{27}$/CB	39.00	2.95	2.98	2.6
$Au_{59}Rh_{41}$/CB	39.25	3.84	2.30	2.2
$Au_{44}Rh_{56}$/CB	39.67	3.75	2.35	2.4
$Au_{27}Rh_{73}$/CB	39.72	4.21	2.10	2.3
$Au_{23}Rh_{77}$/CB	40.28	5.12	1.73	2.2
Rh/CB	41.41	5.35	1.66	1.9

[a]The data were the same in Fig. 3h.

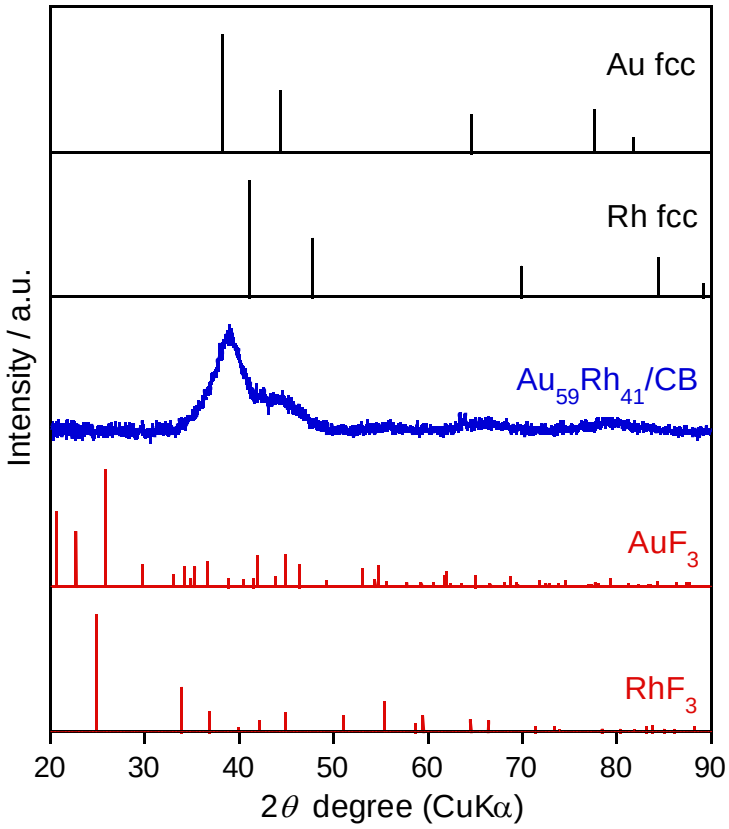

Figure S3. An XRD pattern of $Au_{59}Rh_{41}$/CB catalyst in a wide range of diffraction angle. The result is the same as shown in Fig. 4a. Standard diffraction patterns of Au, Rh, AuF_3, and RhF_3 (PDF file# 00-004-0784, 00-005-0685, 01-085-2315, and 01-078-1122, respectively) are also shown.

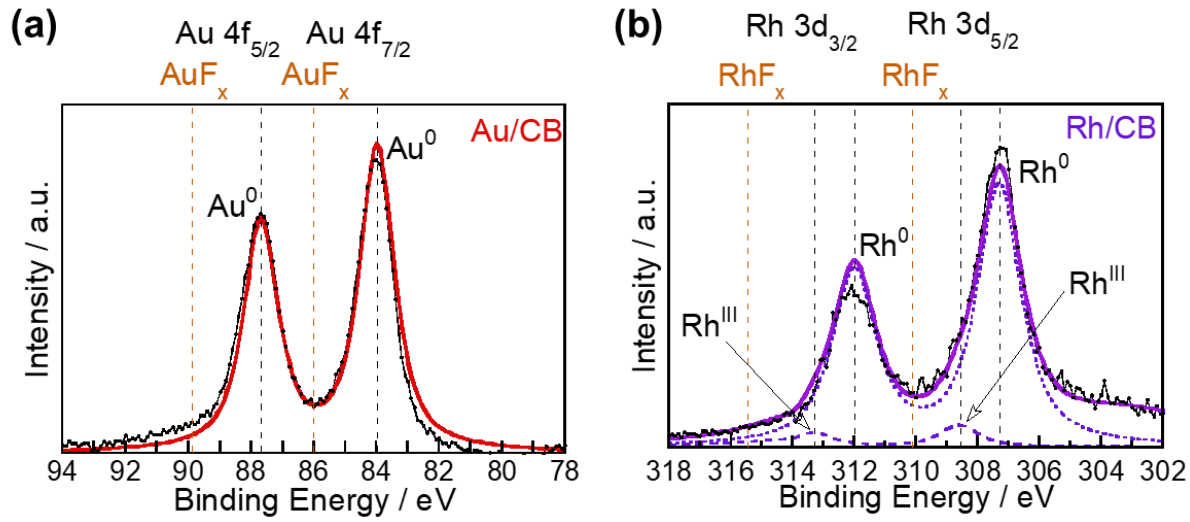

Figure S4. XPS spectra for (a) Au 4f of Au/CB and (b) Rh 3d of Rh/CB. The obtained spectra showed no signals of metal fluorides, which showed Au $4f_{5/2}$ and $4f_{7/2}$ peaks at 89.9 eV and 86.0 eV, respectively, for AuF_x and Rh $3d_{3/2}$ and $3d_{5/2}$ peaks at 315.5 eV and 310.2 eV, respectively, for RhF_x.[S1]

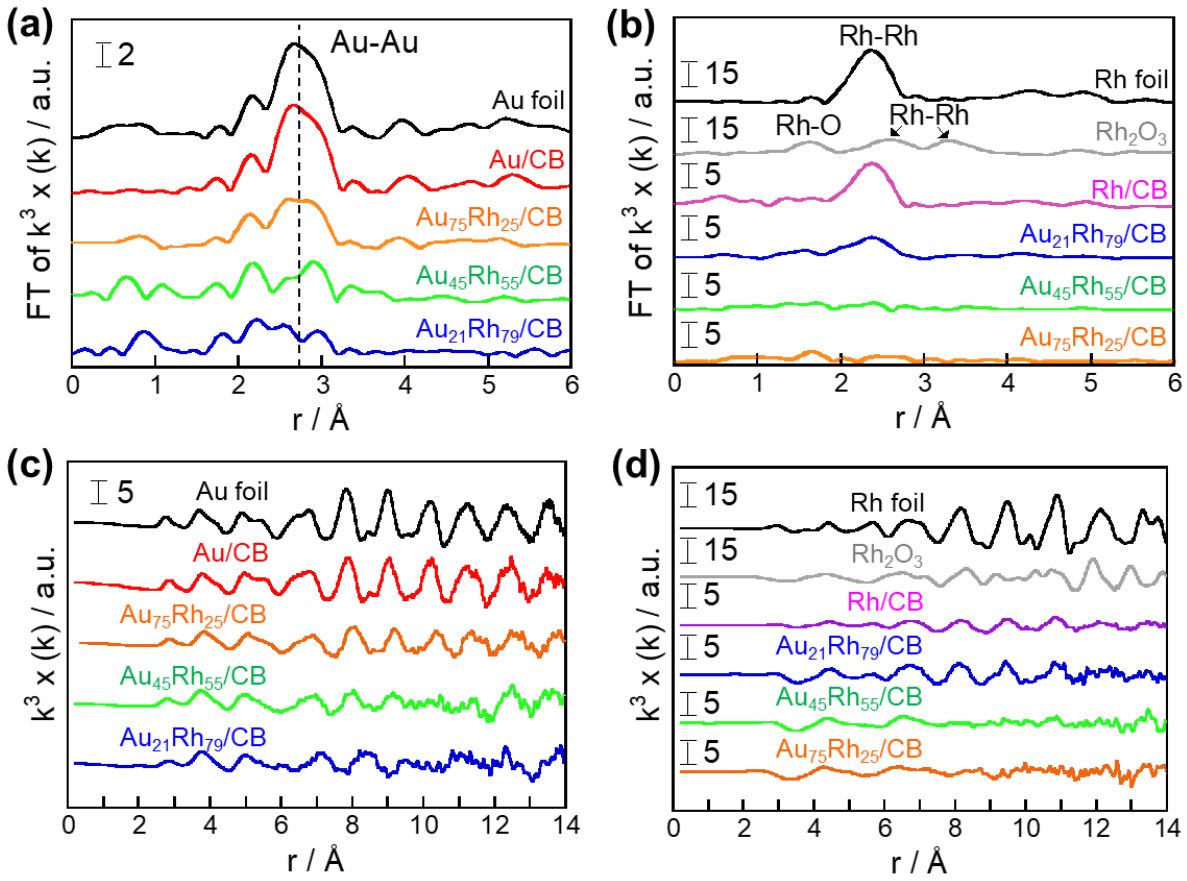

Figure S5. Fourier-transformed extended X-ray absorption fine structures (FT-EXAFS) spectra and k^3-weighted EXAFS oscillation at the Au L_3-edge (a, c) and the Rh K-edge (b, d) of Au/CB, $Au_{75}Rh_{25}$/CB, $Au_{45}Rh_{55}$/CB, $Au_{21}Rh_{79}$/CB, and Rh/CB in reference to the standard Au foil, Rh foil and Rh_2O_3.

Table S2. Results of the curve-fitting analysis for Au L_3-edge and Rh K-edge FT-EXAFS.

sample	bond	C. N. [a]	C. N. sum	R (Å)	D. W. [b]	R factor (%) [c]
Au foil	Au-Au	11.5 (3)	11.5	2.85 (2)	0.091 (15)	8.5
Au/CB	Au-Au	9.4 (3)	9.4	2.85 (2)	0.088 (16)	10.1
$Au_{75}Rh_{25}$/CB	Au-Au	8.2 (3)	8.8	2.82 (3)	0.096 (19)	7.3
	Au-Rh	0.6 (2)		2.79 (6)	0.087 (47)	
$Au_{45}Rh_{55}$/CB	Au-Au	5.9 (3)	7.6	2.82 (3)	0.087 (19)	8.8
	Au-Rh	1.7 (2)		2.80 (4)	0.085 (27)	
$Au_{21}Rh_{79}$/CB	Au-Au	2.5 (3)	7.6	2.83 (4)	0.085 (29)	12.6
	Au-Rh	5.1 (3)		2.78 (3)	0.105 (21)	
Rh foil	Rh-Rh	11.0 (1)	11.0	2.69 (1)	0.064 (77)	12.3
Rh_2O_3	Rh-Rh	1.8 (1)	6.0	2.82 (2)	0.022 (23)	13.5
	Rh-O	4.2 (2)		2.04 (2)	0.040 (23)	
Rh/CB	Rh-Rh	5.3 (2)	6.9	2.68 (2)	0.084 (14)	13.0
	Rh-O	1.6 (3)		2.06 (8)	0.110 (55)	

The numbers in parentheses are the uncertainties, for example, 9.4 (3) represents 9.4 ± 0.3.

[a] Coordination number.

[b] Debye–Waller factor.

[c] R factor = $\left(\sum\left(k^3X^{exp}(k) - k^3X^{fit}(k)\right)^2\right)^{1/2} \Big/ \left(\sum\left(k^3X^{exp}(k)\right)^2\right)^{1/2}$.

For smaller sized metal nanoparticles, the amplitude of the M-M bond was decreased due to the large effect of thermal fluctuation, resulting in a relatively large R factor, as previously reported for small metal clusters in the literature (Yamazoe, *et al*., *Nat. Commun*., 2016, **7**, 10414).

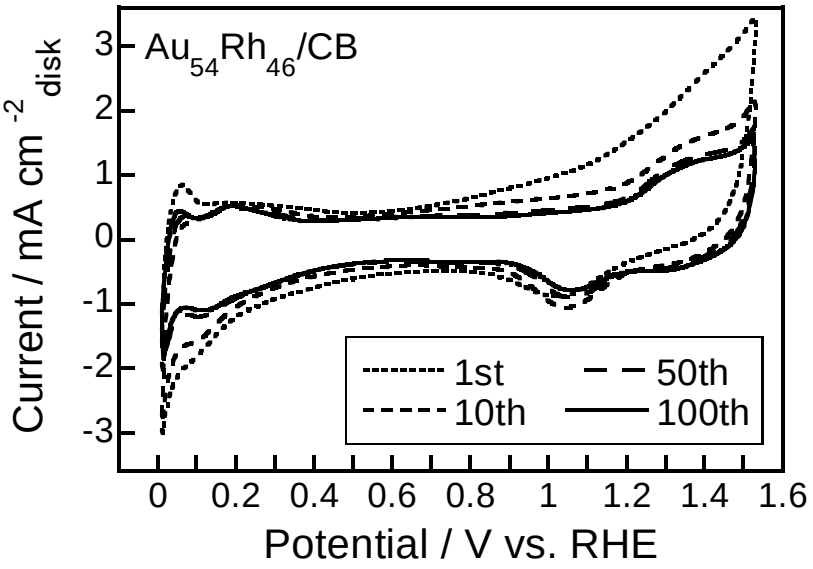

Figure S6. Representative cyclic voltammograms of $Au_{54}Rh_{46}$/CB on GC disk electrode in an N_2-saturated 0.50 mol dm^{-3} KOH solution with a potential scan rate of 0.10 V s^{-1} at different numbers of potential sweep cycles.

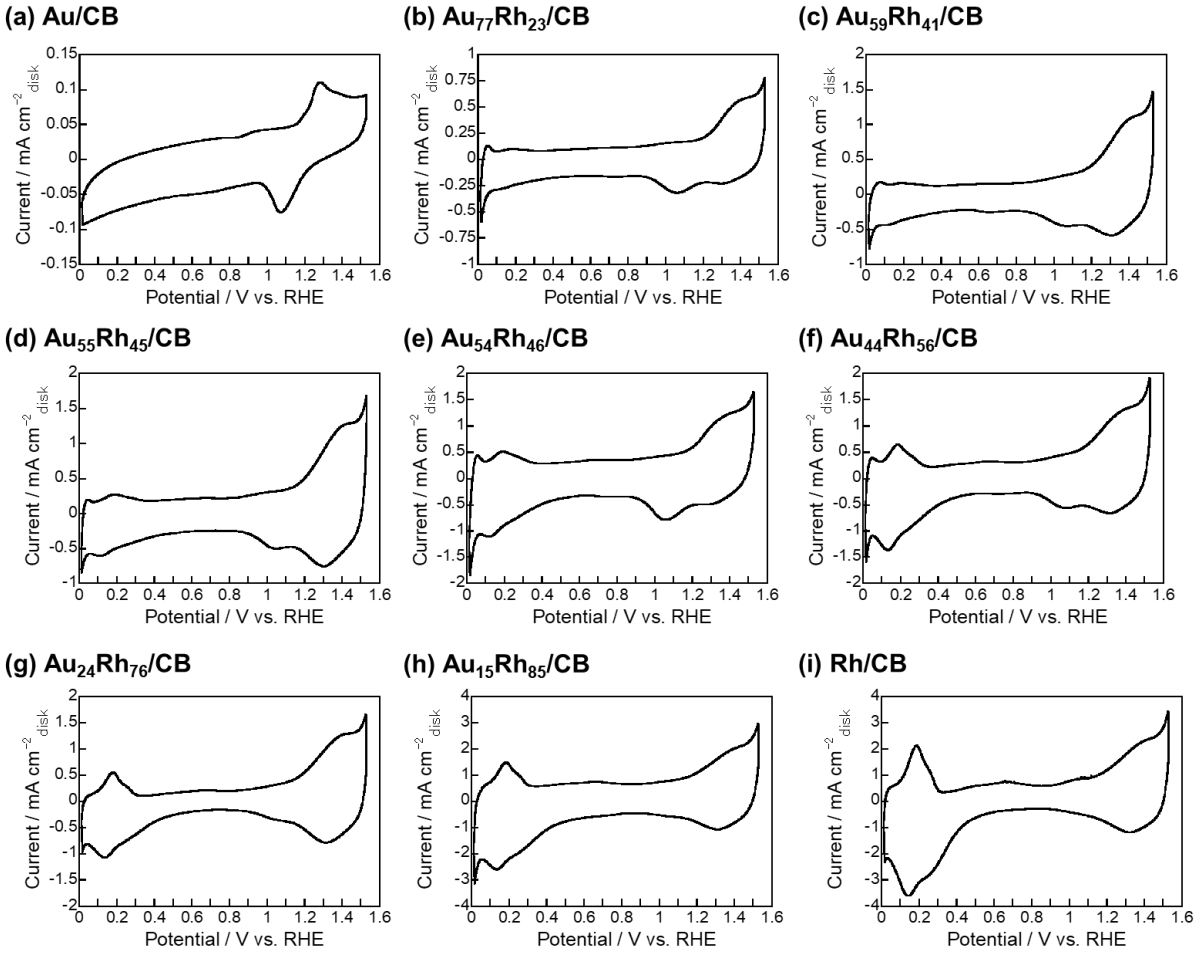

Figure S7. Cyclic voltammograms of AuRh/CB immobilized on the GC disk electrode in an N_2-saturated 0.50 mol dm^{-3} KOH solution with a potential scan rate of 0.10 V s^{-1}. The samples were Au/CB (a), $Au_{77}Rh_{23}$/CB (b), $Au_{59}Rh_{41}$/CB (c), $Au_{55}Rh_{45}$/CB (d), $Au_{54}Rh_{46}$/CB (e), $Au_{44}Rh_{56}$/CB (f), $Au_{24}Rh_{76}$/CB (g), $Au_{15}Rh_{85}$/CB (h), and Rh/CB (i).

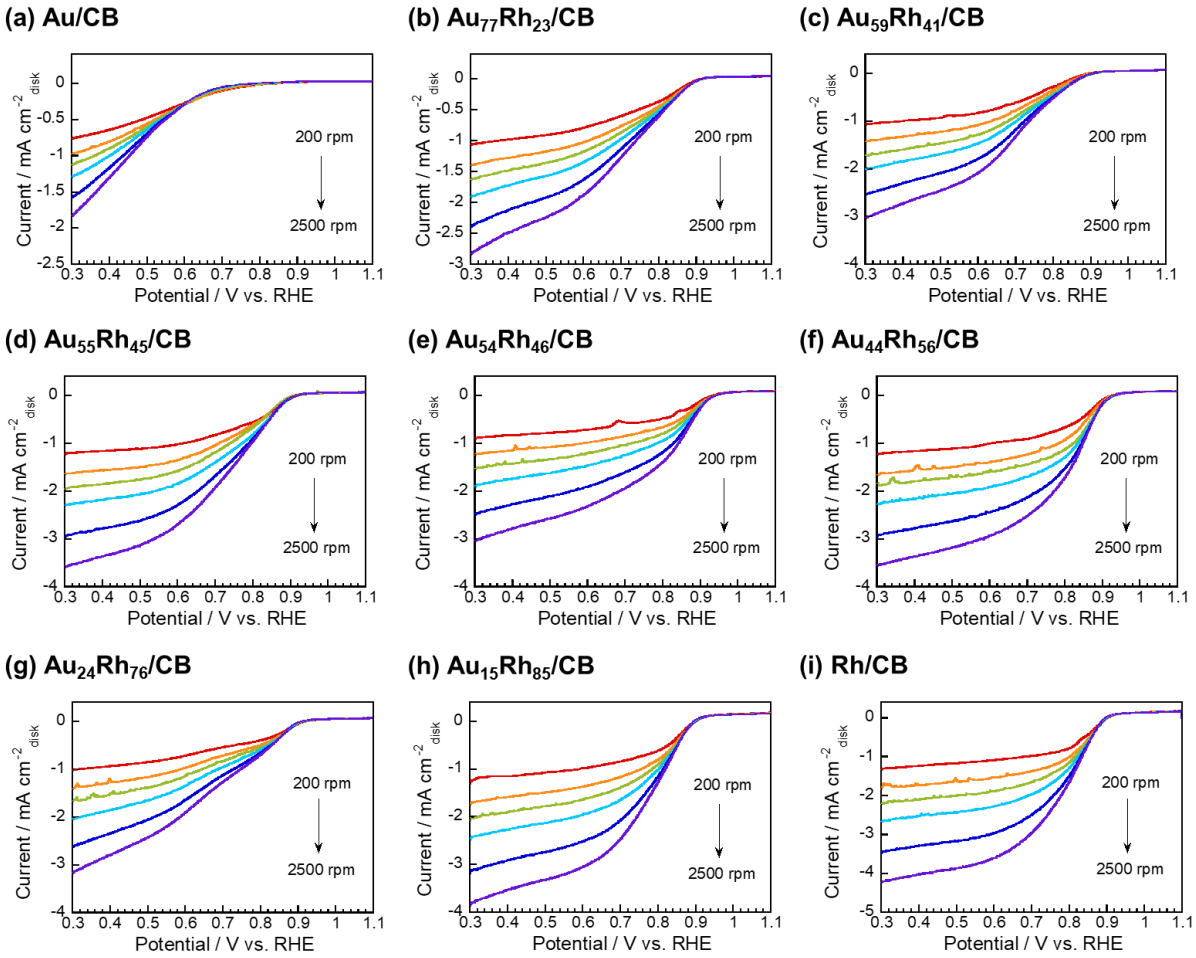

Figure S8. Hydrodynamic voltammograms of RRDE with an AuRh/CB-loaded GC disk in an O_2-saturated 0.50 M KOH aqueous solution under the rotation speed of 200−2500 rpm. The disk potential was scanned at a rate of 0.02 V s^{-1}. The catalysts used were Au/CB (a), $Au_{77}Rh_{23}$/CB (b), $Au_{59}Rh_{41}$/CB (c), $Au_{55}Rh_{45}$/CB (d), $Au_{54}Rh_{46}$/CB (e), $Au_{44}Rh_{56}$/CB (f), $Au_{24}Rh_{76}$/CB (g), $Au_{15}Rh_{85}$/CB (h), and Rh/CB (i). The disk currents were normalized by the geometric areas of their electrodes.

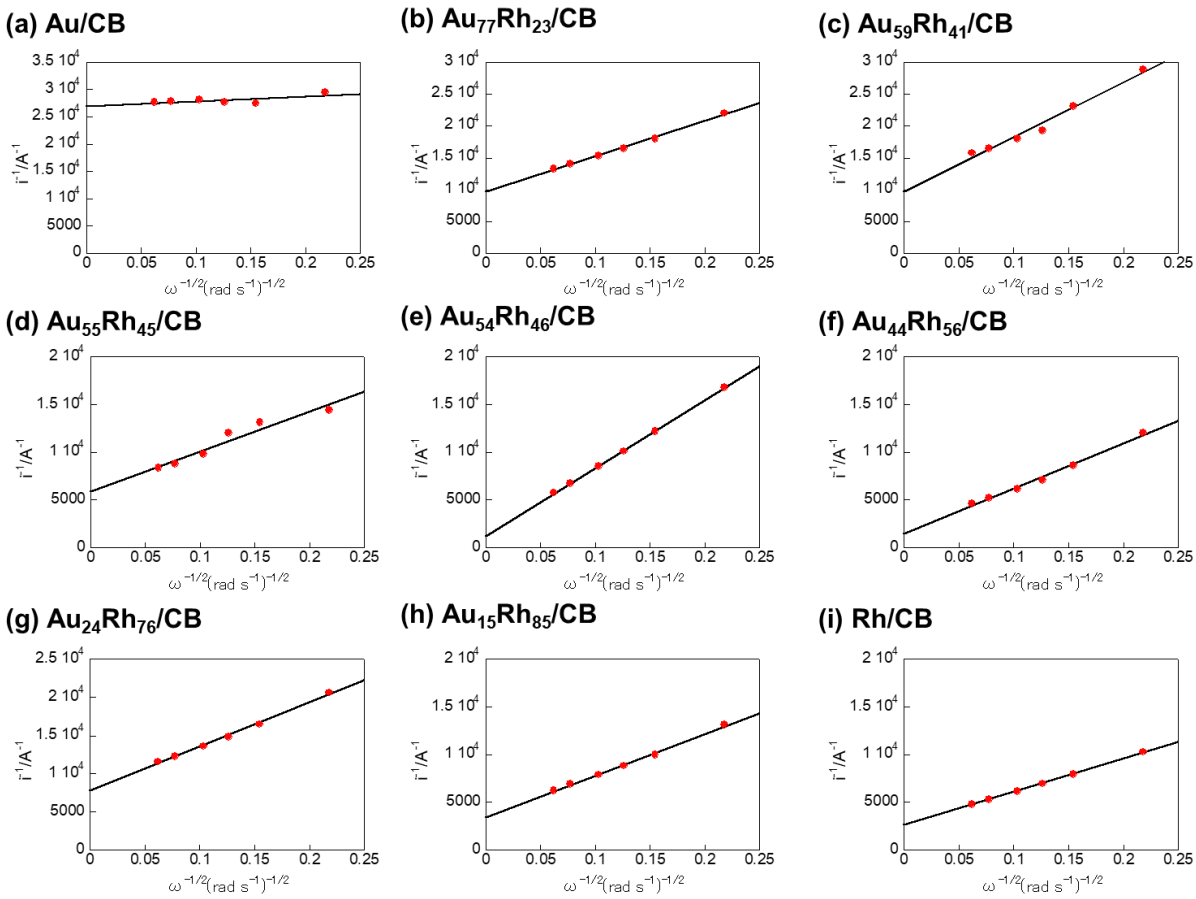

Figure S9. Koutecky-Levich plots of the current at +0.60 V vs. RHE for Au/CB (a) and the currents measured at +0.80 V vs. RHE for AuRh/CB (b-h) and Rh/CB (i). The results shown in Fig. S8 were used for the calculation.

Reference

(S1) A. Tressaud and P. Hagenmuller, *J. Fluorine Chem*., 2001, **111**, 221.